



ELSEVIER



BASIC SCIENCE

Nanomedicine: Nanotechnology, Biology, and Medicine  
17 (2019) 106–118



nanomedjournal.com

Original Article

# Engineered Relaxin as theranostic nanomedicine to diagnose and ameliorate liver cirrhosis

Beata Nagórniwicz, MSc<sup>a</sup>, Deby F. Mardhian, MSc<sup>a</sup>, Richell Booijink, MSc<sup>a</sup>,  
Gert Storm, PhD<sup>a,b</sup>, Jai Prakash, PhD<sup>a,1</sup>, Ruchi Bansal, PhD<sup>a,\*,1</sup>

<sup>a</sup>Department of Biomaterials Science and Technology, Technical Medical Centre, Faculty of Science and Technology, University of Twente, Enschede, The Netherlands

<sup>b</sup>Department of Pharmaceutics, Utrecht Institute of Pharmaceutical Sciences, Faculty of Science, Utrecht University, Utrecht, The Netherlands

Revised 17 December 2018

## Abstract

Hepatic cirrhosis is a growing health problem with increasing mortality worldwide. So far, there is a lack of early diagnosis and no clinical therapy is approved for the treatment. In this study, we developed a novel theranostic nanomedicine by targeting relaxin (RLX) that is known to possess potent anti-fibrotic properties but simultaneously has poor pharmacokinetics and detrimental off-target effects. We conjugated RLX to PEGylated superparamagnetic iron-oxide nanoparticles (RLX-SPIONs) and examined hepatic stellate cells (HSCs) specific binding/uptake. Thereafter, we assessed the therapeutic efficacy of RLX-SPIONs on human HSCs in vitro and in vivo in CCl<sub>4</sub>-induced liver cirrhosis mouse model. RLX-SPIONs showed specific binding and uptake in TGFβ-activated HSCs, and inhibited TGFβ-induced HSCs differentiation, migration and contraction. In vivo, RLX-SPIONs strongly attenuated cirrhosis and showed enhanced contrast in MR imaging. Altogether, this study presents RLX-SPIONs as a novel theranostic nanomedicine that provides new opportunities for the diagnosis and treatment of liver cirrhosis.

© 2019 The Authors. Published by Elsevier Inc. This is an open access article under the CC BY-NC-ND license (<http://creativecommons.org/licenses/by-nc-nd/4.0/>).

**Key words:** Relaxin; Superparamagnetic iron-oxide nanoparticles (SPIONs); Hepatic stellate cells; Cirrhosis; Theranostics; Nanomedicine

Liver cirrhosis remains the growing cause of increasing morbidity and mortality worldwide with no clinically approved therapy.<sup>1–3</sup> Cirrhosis is a chronic disease that develops after a chronic injury over more than 20 years. There are two major clinical challenges in the management of this disease; the first is the diagnosis for monitoring the progression of the disease using non-invasive methods and the second is the therapeutic treatment which

is effective at the chronic disease stage. There are several endogenous compounds secreted locally in nanograms and are highly potent in inhibiting fibrogenesis, however often elicit off-target adverse effects when administered systemically.<sup>4</sup> Therefore, their therapeutic applicability for the long-term treatment of chronic diseases is not realistic. In earlier studies, we have engineered an endogenous cytokine interferon gamma, that possess potent anti-

**Abbreviations:** ECM, extracellular matrix; RLX, relaxin; SPIONs, superparamagnetic iron-oxide nanoparticles; RLX-SPIONs, relaxin coated superparamagnetic iron-oxide nanoparticles; HSCs, hepatic stellate cells; CCl<sub>4</sub>, carbon tetrachloride; TGFβ, transforming growth factor beta; qRT-PCR, quantitative reverse transcription–polymerase chain reaction; Col1a1, collagen-I; Des, desmin; α-SMA, alpha smooth muscle actin; Timp1, tissue inhibitor of matrix metalloproteases 1; MMP, matrix metalloprotease; CD, cluster of differentiation; HIF-1α, hypoxia inducing factor 1 alpha; ALT, alanine aminotransferase; MRI, Magnetic resonance imaging.

**Conflict of Interest:** The authors declare no competing financial interest.

**Acknowledgments:** This project was supported by the Netherlands Organization for Health Research and Development (ZonMW, NWO)-funded VENI innovation grant 916.151.94 (to R.B.). Authors thank B. Klomphaar for the technical assistance during the animal experiments. We also acknowledge A. Veltien for MRI measurements and Prof. A. Heerschap for discussion and expert opinion for MRI.

\*Corresponding author at: Department of Biomaterials Science and Technology, University of Twente, 7500 AE Enschede, The Netherlands.

E-mail address: [r.bansal@utwente.nl](mailto:r.bansal@utwente.nl) (R. Bansal).

<sup>1</sup> Equal contribution.

<https://doi.org/10.1016/j.nano.2018.12.008>

1549-9634/© 2019 The Authors. Published by Elsevier Inc. This is an open access article under the CC BY-NC-ND license (<http://creativecommons.org/licenses/by-nc-nd/4.0/>).

Please cite this article as: Nagórniwicz B, et al. Engineered Relaxin as theranostic nanomedicine to diagnose and ameliorate liver cirrhosis. *Nanomedicine: NBM* 2019;17:106–118, <https://doi.org/10.1016/j.nano.2018.12.008>

fibrotic properties but with immune-related off-target effects, with a targeting peptide and demonstrated improved therapeutic efficacy and no off-target effects.<sup>5–7</sup>

Relaxin (RLX), an endogenous two-chain peptide hormone structurally similar to insulin, is an anti-fibrotic hormone that has been shown to be therapeutically effective in liver, kidney and heart cirrhosis, and progressive systemic sclerosis.<sup>8–16</sup> RLX binds and activates G-protein coupled receptor, relaxin family peptide receptor 1 (RXFP1). While RLX has emerged as a potential therapeutic in several diseases, RLX has a very short half-life due to small size (6KDa) and rapid renal clearance,<sup>17,18</sup> therefore chronic administration in fibrotic diseases i.e. continuous infusion (via osmotic pumps) increase systemic vasodilation<sup>19</sup> therefore poses hindrance for the clinical translation.

Superparamagnetic iron-oxide nanoparticles (SPIONs) are promising nanoparticles with unique magnetic properties and tailored surface chemistry that facilitated their clinical application for magnetic resonance imaging (MRI) and drug targeting.<sup>20–22</sup> SPIONs possess excellent physiochemical properties such as magnetization with negligible remanence, colloidal stability, low cytotoxicity, and therefore has huge potential for biomedical applications.<sup>23,24</sup> Recent developments of polymer (dextran/PEG)-coated SPIONs has shown tremendous improvements in biocompatibility and blood circulation. Ferumoxide (dextran-coated SPIONs, Ferridex) and Ferucarbotran (carboxydextran-coated SPION, Resovist) are the two clinically approved SPIONs for liver cancer imaging.<sup>25</sup>

In the present study, we conjugated RLX on the surface of dextran-coated SPIONs to target to the fibrotic livers to achieve localized anti-fibrotic efficacy with reduced off-target systemic effects. In addition, use of SPIONs provided a great opportunity for diagnosing cirrhosis. We first confirmed the overexpression of RLX receptor RXFP1 in hepatic stellate cells (HSCs), the key fibrogenic cells in liver cirrhosis, in CCl<sub>4</sub>-induced liver cirrhosis mouse model and human pathological fibrotic liver tissues. We then conjugated RLX on SPIONs chemically at lysine present in RLX. RLX-SPIONs were characterized and investigated for their binding and activity in vitro in HSCs. In vivo in CCl<sub>4</sub>-induced liver cirrhosis in mice, we examined the liver distribution of RLX-SPIONs using MRI and investigated the therapeutic efficacy following post-disease treatment. To our best knowledge, this is the first study documenting a theranostic nanomedicine based on RLX, especially to HSCs in liver, for MRI-based diagnosis and treatment of liver cirrhosis.

## Methods

### Conjugation of Relaxin to SPIONs

Conjugation of Human Relaxin-2 (H2-RLX or RLX, Pepro-Tech, Rocky Hill, NJ) to SPIONs (micromod Partikeltechnologie, GmbH, Rostock, Germany) was performed using carbodiimide chemistry (**Supplementary Fig. 1**). Briefly, 100 µL of SPIONs (5 mg/ml) were activated with 10 µmol EDC (1-ethyl-3-(3-dimethylaminopropyl)-carbodiimide HCl, Sigma, St. Louis, MO, USA) and 35 µmol NHS (N-hydroxysuccinimide, Sigma) prepared in 125 µL of MES [2-(N-morpholino) ethanesulfonic acid, Sigma] buffer (pH 6.3). After 45 min, samples were purified with 30KDa

Amicon® Ultra Centrifugal Filters (Merck Millipore, Darmstadt, Germany). 5 µg of RLX (0.8 nmol in 10 µL) was added to the activated SPIONs and reacted overnight at 4 °C. Samples were purified and unconjugated COOH groups (on SPIONs) were reacted with glycine (Sigma) for 30 min at RT. Finally, relaxin-coated SPIONs (RLX-SPIONs) were purified and stored at 4 °C.

### Characterization of RLX-SPIONs

SPIONs and RLX-SPIONs size were measured by dynamic light scattering (DLS) using Zetasizer Nano (Malvern Instruments, UK). Conjugation efficiency of RLX on SPIONs was determined by Dot-Blot analysis. Briefly, SPIONs, RLX and RLX-SPIONs were serially diluted in TBS buffer (Thermo Scientific, Rockford, IL, USA) and 5 µL of samples were spotted on the nitrocellulose membrane and blocked for 1 h in 5% blotting-grade blocker (Bio-Rad, Hercules, CA, USA) prepared in Tween®-20 TBS buffer (TTBS; Thermo Scientific). Membrane was incubated with rat anti-H2-RLX monoclonal antibody (1:1000; R&D Systems, Minneapolis, MN, USA) for 1 hr. Membrane was washed in TTBS and incubated for 1 h with secondary rabbit anti-rat polyclonal antibody (1:1000, Dako, Glostrup, Denmark) followed by tertiary polyclonal goat-anti rabbit antibody (1:1000, Dako). Finally, blot was developed using Pierce® ECL Plus Western Blotting Substrate (Thermo Scientific) and imaged using FluorChem Imaging System (ProteinSimple, Alpha Innotech, San Leandro, CA, USA). To estimate loss of SPIONs during conjugation process, Prussian blue iron-staining (Sigma) as per manufacturer's instructions was performed on the dot blots. The dots were quantified using NIH ImageJ software (NIH, Bethesda, MD) and the conjugation efficiency was calculated using the standard curves prepared from RLX and SPIONs dots (with known concentrations) as presented in **Supplementary Fig. 2**. The conjugation efficiency as determined from the standard curves from dot-blot and Prussian blue staining's was found to be 90% that corresponded to three RLX peptides per SPION.

### Cell lines

Human hepatic stellate cells (LX2 cells), immortalized human-derived cell line, provided by Prof. Scott Friedman (Mount Sinai Hospital, New York, NY, USA) were cultured in DMEM-Glutamax (Invitrogen, Carlsbad, CA, USA) supplemented with 10% fetal bovine serum (FBS, Lonza) and antibiotics (50 U/ml Penicillin and 50 µg/ml streptomycin, Sigma). Murine NIH3T3 fibroblasts were obtained from American Type Culture Collection (ATCC, Manassas, VA, USA) and were cultured in Dulbecco's modified Eagle's (DMEM) medium (Lonza) supplemented with 10% FBS and 2 mM L-glutamine (Sigma) and antibiotics.

### Cell binding and uptake experiments

LX2 cells were seeded at  $1 \times 10^4$  cells/well and cultured overnight. Cells were serum-starved and incubated with TGFβ1 (Roche, Mannheim, Germany) for 24 h. TGFβ-activated LX2 cells were incubated with SPIONs and RLX-SPIONs at RT for 2 h (binding study) or at 37 °C for 4 h (uptake study) in with 0.5% BSA supplemented medium. After incubation, cells were washed thrice and were fixed with 4% formalin and stained using Prussian Blue iron staining as per manufacturer's instructions and imaged

using Hamamatsu NanoZoomer Digital slide scanner 2.0HT (Hamamatsu Photonics, Bridgewater NJ). Cellular uptake was assessed by counting iron-positive cells/per field with which % uptake was calculated.

### 3D collagen-I gel contraction assay

A collagen suspension (5 ml) containing 3 ml of collagen G1 (5 mg/ml, Matrix biosciences, Morlenbach, Germany), 0.5 ml of 10x M199 medium (Sigma), 85 µl of 1 N NaOH (Sigma) and sterile water was mixed with 1 ml ( $2 \times 10^6$ ) of LX2 cells. The gel and cell suspension (0.6 ml/well) was plated in a 24-well culture plate and was allowed to polymerize. Polymerized gels were incubated with 1 ml of 0.5% FBS-containing medium with or without human recombinant TGFβ (5 ng/ml) together with 1 µg/ml of RLX, RLX-SPIONs and SPIONs (equimolar concentration), followed by detachment of the gels. The size of the gels were digitally measured and normalized with their respective well size in each image.

### Cell migration/wound healing experiments

Cells were plated in 12-well culture plates ( $1 \times 10^5$  cells/well), cultured overnight and serum-starved for 24 h. A standardized scratch was made using a 200 µl pipette tip fixed in a holder. Cells were then washed twice and were incubated with starvation medium (control), or with 5 ng/ml TGFβ with and without 1 µg/ml RLX, SPIONs and RLX-SPIONs. To measure the migration, microscopic photographs were taken at 0 and 24 h. Images were analyzed using NIH ImageJ software and were represented as % wound closure relative to the control wells.

### In vitro effect studies of RLX and RLX-SPIONs

Cells were seeded in 24-well plates ( $3 \times 10^4$  cells/well for staining) and 12-well plates ( $8 \times 10^4$  cells/well for quantitative PCR analysis and western blot analysis). Cells were serum-starved and incubated with starvation medium alone, 1 µg/ml RLX, SPIONs and RLX-SPIONs, and 5 ng/ml TGFβ1 for 24 h. Cells (24-well plates) were then fixed and stained for collagen I and α-SMA (refer to Supplementary **Table 1**). In addition, cells (12-well plates) were lysed either with protein lysis buffer or RNA lysis buffer for subsequent analyses.

We also performed the in vitro effect studies with and without serum (2%) to investigate the effect of serum on the stability of RLX and RLX-SPIONs. Cells were seeded in 12-well plates ( $8 \times 10^4$  cells/well for staining). Cells were serum-starved for 24 h after which the standardized scratches were made. The cells were then incubated with medium (with and without serum) alone, 1 µg/ml RLX, SPIONs and RLX-SPIONs, and 5 ng/ml TGFβ1 for 24 h. Images were made at  $t = 0$  h and  $t = 24$  h to analyze the cell migration. Images were analyzed using NIH ImageJ software and were represented as % wound closure relative to the control wells. Cells were lysed either with RNA lysis buffer for subsequent analyses.

### CCl<sub>4</sub>-induced advanced liver cirrhosis mouse model

All the animal experiments were performed in strict accordance with the ethical guidelines for the Care and Use of Laboratory Animals, Utrecht University, The Netherlands. Male

Balb/c mice (8–10 weeks old;  $n = 5$  per group) were treated with intra-peritoneal injections with olive oil or 1 ml/kg carbon tetrachloride (CCl<sub>4</sub>, Sigma), prepared in olive oil (Sigma) twice weekly for 8 weeks as described elsewhere.<sup>7</sup> In the last 2 weeks, CCl<sub>4</sub>-treated mice received intravenous administration of PBS ( $n = 6$ ), RLX (250 ng/dose,  $n = 6$ ), RLX-SPIONs (250 ng/dose,  $n = 6$ ) and SPIONs (equimolar concentrations,  $n = 5$ ) three times a week (in total 6 intravenous injections). Healthy controls ( $n = 5$ ) received olive oil for 8 weeks. Finally, all the animals were euthanized, and liver tissues, and blood samples were collected for subsequent analysis.

### Magnetic resonance imaging

For MRI, Balb/c mice with 8 weeks of CCl<sub>4</sub> administration were intravenously injected with 5 µg/dose RLX, RLX-SPIONs and SPIONs (equimolar concentrations) 30 min before imaging. MRI measurements were performed on a BioSpec Avance III small animal MR system (Bruker BioSpin, Ettlingen, Germany) equipped with an shielded gradient set of 600mT/m operating on Paravision 5.1 software platform (Bruker, Karlsruhe, Germany). First gradient echo T2\*-weighted images covering the entire mouse liver were acquired in three directions for anatomical reference using described acquisition parameters.

### Immunohistochemistry and Immunofluorescence

Liver tissues were harvested and transferred to Tissue-Tek OCT embedding medium (Sakura Finetek, Torrance, CA, USA) and snap-frozen in 2-methyl butane. Cryosections (4 µm) were air-dried and fixed with acetone for 10 min. Cells or tissue sections were rehydrated with PBS and incubated with the primary antibody (refer to Supplementary **Table 1**) followed by incubation with horseradish peroxidase (HRP)-conjugated secondary antibody. Next, the samples were incubated with HRP-conjugated tertiary antibody or donkey anti-goat Alexa 594-labeled tertiary antibody (Life Technologies, Gaithersburg, MD, USA). Thereafter, peroxidase activity was developed using the AEC (3-amino-9-ethyl carbazole) substrate kit (Life Technologies) for 20 min, and nuclei were counterstained with hematoxylin (Fluka Chemie, Buchs, Switzerland). For tissue sections, endogenous peroxidase activity was blocked by 3% H<sub>2</sub>O<sub>2</sub> prepared in methanol. Cells or sections were mounted with Aquatex mounting medium (Merck, Darmstadt, Germany) or DAPI-containing mounting medium (Sigma). The staining was visualized and the images were captured using light microscopy (Nikon eclipse E600 microscope, Tokyo, Japan).

### Western blot analysis

Cells were homogenized in cold RIPA buffer [with protease inhibitor and phosphatase inhibitor (Roche)] and centrifuged at 12,000 rpm for 1 h at 4 °C. The samples were subjected to SDS-PAGE with 10% Tris-glycine gels (Life Technologies) followed by transfer to PVDF membrane. The membranes were developed according to the standard protocols using primary and secondary antibodies as mentioned in Supplementary **Table 1**. The bands were visualized using ECL detection reagent (PerkinElmer) and photographed using FluorChem Imaging System. Intensity of



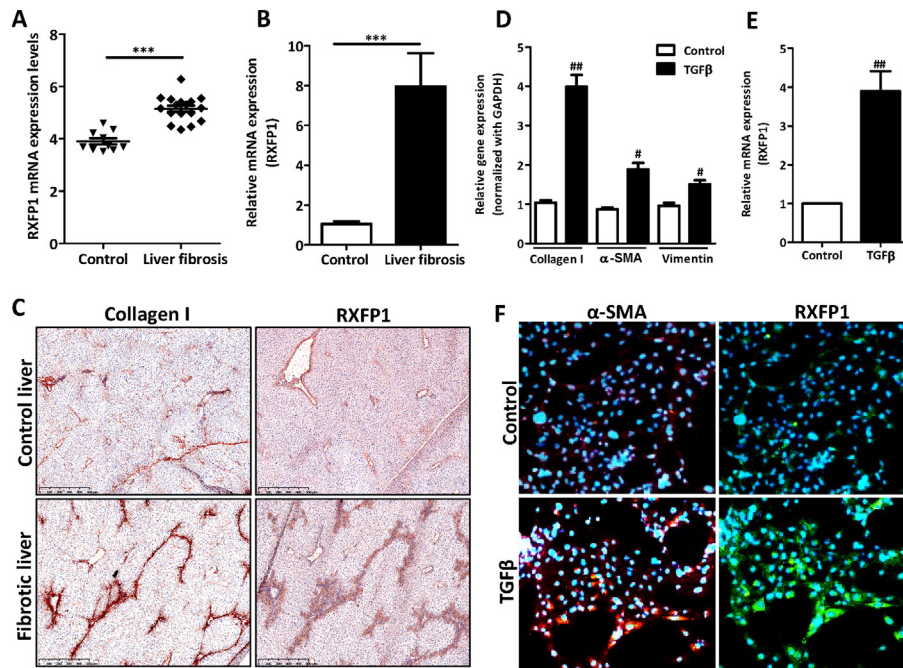


Figure 1. Up-regulation of RXFP1 in fibrotic human livers, CCl<sub>4</sub>-induced chronic liver cirrhosis in mice and TGFβ-activated hepatic stellate cells. (A) RXFP1 mRNA expression levels from publicly available transcriptome profiling datasets. The graph depicts RXFP1 mRNA expression in liver tissues from HBV-infected liver cirrhosis (n = 17) as compared to controls (n = 10). (B) mRNA expression of RXFP1 in the livers of olive-oil-treated control mice and CCl<sub>4</sub>-treated fibrotic mice (8 weeks). n = 5 per group. \*\*\*P < 0.001 denotes significance versus control. (C) Collagen I- and RXFP1-stained liver sections from control livers and CCl<sub>4</sub>-treated fibrotic mice (n = 5). (D) Gene expression of fibrotic parameters (Collagen I, α-SMA and vimentin), and (E) RXFP1 in control and TGFβ-activated LX2 cells, n = 4. #P < 0.05 and ##P < 0.01 denotes significance versus control cells. (F) Representative images showing α-SMA and RXFP1 expression in control and TGFβ-activated LX2 cells.

individual bands was quantified using NIH ImageJ software and expressed in % relative to β-actin.

#### RNA extraction, reverse transcription and quantitative real-time PCR

Total RNA from cells and liver tissues was isolated using the GenElute Total RNA Miniprep Kit (Sigma) and SV total RNA isolation system (Promega Corporation, Madison, WI, USA), respectively, according to manufacturer's instructions. The RNA concentration was quantitated and total RNA (1 μg) was reverse transcribed using the iScript cDNA Synthesis Kit (Bio-Rad, Hercules, CA, USA). Real-time PCR was performed using the 2x SensiMix SYBR and Fluorescein Kit (Bioline GmbH, QT615–05, Luckenwalde, Germany), 20 ng of cDNA and pre-tested gene-specific primer sets (listed in **Supplementary Tables 2 and 3**) according to manufacturer's instructions. Finally, cycle threshold (Ct) values were normalized to the reference gene GAPDH, and relative expression were calculated using the  $2^{-\Delta\Delta C_t}$  method.

#### RXFP1 gene expression in the human cohort from the public database

RXFP1 gene expression was assessed in the publicly available transcriptome datasets of liver tissue from cirrhosis patients with Hepatitis B virus infection (n = 10 controls; n = 17 liver cirrhosis, GSE38941) obtained from the National Center for Biotechnology Information Gene Expression Omnibus database (GEO).

#### Statistical analyses

The results are expressed as the mean + standard error of the mean. The graphs and statistical analyses were performed using GraphPad Prism version 5.02 (GraphPad Prism, La Jolla, CA, USA). Multiple comparisons between different groups were performed using the one-way analysis of variance (ANOVA) with the Bonferroni post hoc test. P < 0.05 was considered significant.

#### Results

##### Up-regulation of RLX receptor (RXFP1) expression in HSCs in liver cirrhosis

In this study, we used RLX receptor as HSCs-specific target receptor which is overexpressed on HSCs during liver cirrhosis. Previous studies have demonstrated the hepatic expression of RLX receptor (RXFP1) after carbon tetrachloride (CCl<sub>4</sub>) and bile-duct ligation (BDL) induced liver cirrhosis models, and in explanted end-stage human cirrhotic livers, and in the livers from patients with early and advanced liver cirrhosis due to non-alcoholic steatohepatitis (NASH) and autoimmune hepatitis (AIH).<sup>8,26</sup> Here, we examined RXFP1 mRNA expression in HBV-infected liver cirrhosis patients (GSE38941). We observed highly significant upregulation in RXFP1 mRNA expression in patients with liver cirrhosis as compared to healthy controls (Figure 1, A). Furthermore, we examined the RXFP1 expression

in mouse fibrotic livers as compared to healthy mouse livers. As shown in **Figure 1, B**, RXFP1 expression was strongly induced in CCl<sub>4</sub>-induced liver cirrhosis mouse model (8-weeks CCl<sub>4</sub>) as compared to healthy controls. Repeated administration of CCl<sub>4</sub> in mice for 8-weeks resulted in extensive cirrhosis with an increased deposition of collagen I as shown in **Figure 1, C**. Importantly, expression levels of RXFP1 were correlatively up-regulated and was found to be localized in the areas of cirrhosis (**Figure 1, C**). During fibrogenesis, TGF $\beta$  is one of the key growth factor involved in disease progression by activated fibroblasts.<sup>27,28</sup> Therefore, we investigated the expression levels of RXFP1 in TGF $\beta$ -activated human HSCs (LX2) as compared to non-activated control LX2. As shown in **Figure 1, D**, we observed over-expression of major HSC activation markers ( $\alpha$ -SMA, alpha-smooth muscle actin and vimentin) and collagen I in TGF $\beta$ -activated LX2. Consistent with HSCs markers, RXFP1 expression was significantly upregulated in TGF $\beta$ -activated LX2 (**Figure 1, E**). The protein expression of RXFP1 was also found to be significantly increased in TGF $\beta$ -activated HSCs and the expression was correlated with  $\alpha$ -SMA expressing HSCs (**Figure 1, F**). Altogether, these results suggest the increased RXFP1 mRNA and protein expression in liver cirrhosis patients and in activated HSCs, and therefore suggests RXFP1 as an appropriate therapeutic and diagnostic target.

#### *Synthesis and characterization of relaxin-coated superparamagnetic iron-oxide nanoparticles (RLX-SPIONs)*

We conjugated RLX to COOH groups on the surface on dextran- and PEG-coated SPIONs using carbodiimide chemistry (**Figure 2, A and Supplementary Fig. 1**). **Supplementary Fig. 1** depicts the step-wise reaction to conjugate RLX peptides on COOH functionalized SPIONs. First, carboxyl groups on SPIONs were activated by EDC to form an unstable intermediate product EDC-activated SPIONs. Second, EDC-activated SPIONs were stabilized by NHS followed by coupling with RLX to form RLX-SPIONs with a stable peptide bond. As shown in **Figure 2, B**, RLX conjugation was confirmed by the increase in hydrodynamic size of SPIONs and more negative zeta potential imparted by negatively charged RLX peptides. To estimate conjugation efficiency, dot-blot analysis and Prussian blue staining's were performed, and standard curves were plotted from known concentrations (**Supplementary Fig. 2**). With the standard curves, conjugation efficiency was calculated that indicated the conjugation efficiency of about 90% which corresponded to conjugation of approximately three RLX peptides per SPION (**Figure 2, C**).

#### *Binding and uptake of RLX-SPIONs by TGF $\beta$ -activated HSCs*

As shown earlier, RXFP1 expression was significantly upregulated on TGF $\beta$ -activated HSCs, we performed binding and uptake studies with RLX-SPIONs and SPIONs on TGF $\beta$ -activated HSCs. As shown in **Figure 2, D & E**, RLX-SPIONs showed increased binding and significantly increased uptake in TGF $\beta$ -activated LX2 as compared to unconjugated SPIONs as confirmed by Prussian blue iron staining. RLX-SPIONs uptake was further confirmed by fluorescent RLX staining's where RLX and RLX-SPIONs showed similar binding to TGF $\beta$ -activated LX2 (**Figure 2, F**). These results suggest that RLX

retained RXFP1-mediated binding and uptake following chemical conjugation.

#### *RLX-SPIONs inhibited fibrotic parameters in mouse 3 T3 fibroblasts in vitro*

We further investigated the effects of RLX-SPIONs on TGF $\beta$ -induced 3 T3 fibroblasts activation, migration and TGF $\beta$ -signaling pathway. We first assessed the effect on fibroblasts migration, as shown in **Figure 3, A & B**, RLX and RLX-SPIONs significantly inhibited TGF $\beta$ -induced migration. Thereafter, we examined the effect of RLX-SPIONs on fibrotic parameters and TGF $\beta$ -signaling pathway i.e. phosphorylated SMAD2/3 pathway. We observed significant inhibition in collagen I deposition,  $\alpha$ -SMA expression and TGF $\beta$  signaling pathway following incubation with RLX and RLX-SPIONs (**Figure 3, C & D**). SPIONs had no significant effects on fibroblasts migration, expression of fibrotic parameters and TGF $\beta$ -signaling pathway (**Figure 3, A–D**). These results suggests that RLX retained its anti-fibrotic activity after chemical conjugation to SPIONs. Furthermore, RLX-SPIONs showed improved effects than RLX suggesting increased stability of RLX following conjugation to SPIONs.

#### *RLX-SPIONs inhibited differentiation, migration and contractility of human HSCs (LX2) in vitro*

We then performed studies in immortalized human hepatic stellate (LX2) cells. Following TGF $\beta$ -mediated LX2 activation, we observed significant upregulation of collagen I and  $\alpha$ -SMA protein expression which was significantly inhibited by RLX and RLX-SPIONs (**Figure 4, A**). Consistent with the protein expression, gene expression of major fibrotic parameter i.e. collagen I, and HSCs-activation marker i.e.  $\alpha$ -SMA and TIMP1 (tissue inhibitors of metalloproteinases 1) was highly induced upon TGF $\beta$  activation and strongly reduced with RLX and RLX-SPIONs (**Figure 4, B**). HSCs have been shown to migrate to the sites of tissue injury during fibrogenesis and differentiate into contractile myofibroblasts that promote liver stiffness.<sup>29</sup> Therefore, we examined the effect of RLX and RLX-SPIONs on migration using wound-healing/scratch assays and contractility of LX2 cells using 3D-collagen contraction assay. We found that RLX and RLX-SPIONs significantly inhibited TGF $\beta$ -induced migration of LX2 cells after 24 h (**Figure 4, C & D**). Furthermore, RLX and RLX-SPIONs drastically diminished TGF $\beta$ -induced collagen gel contraction after 24, 48 and 72 h with maximal inhibitory effects observed after 72 h (**Figure 4, E and F**). Altogether, these results suggest RLX retained complete functionality after conjugation on SPIONs.

#### *Magnetic resonance imaging of fibrotic livers using RLX-SPIONs*

We further used RLX-SPIONs for molecular (RXFP1-based) MR imaging in 8-week CCl<sub>4</sub>-induced liver cirrhosis in mice (**Figure 5, A**). Mice were intravenously injected with SPIONs, RLX and RLX-SPIONs 30 min before MR imaging. MRI maps from axial sections of the upper abdomen in T2\* scanning format were made at Tr = 1500 ms and different echo time Te = 8.7 ms, 17.3 ms and 26 ms. T2\* maps of the upper abdomen showed

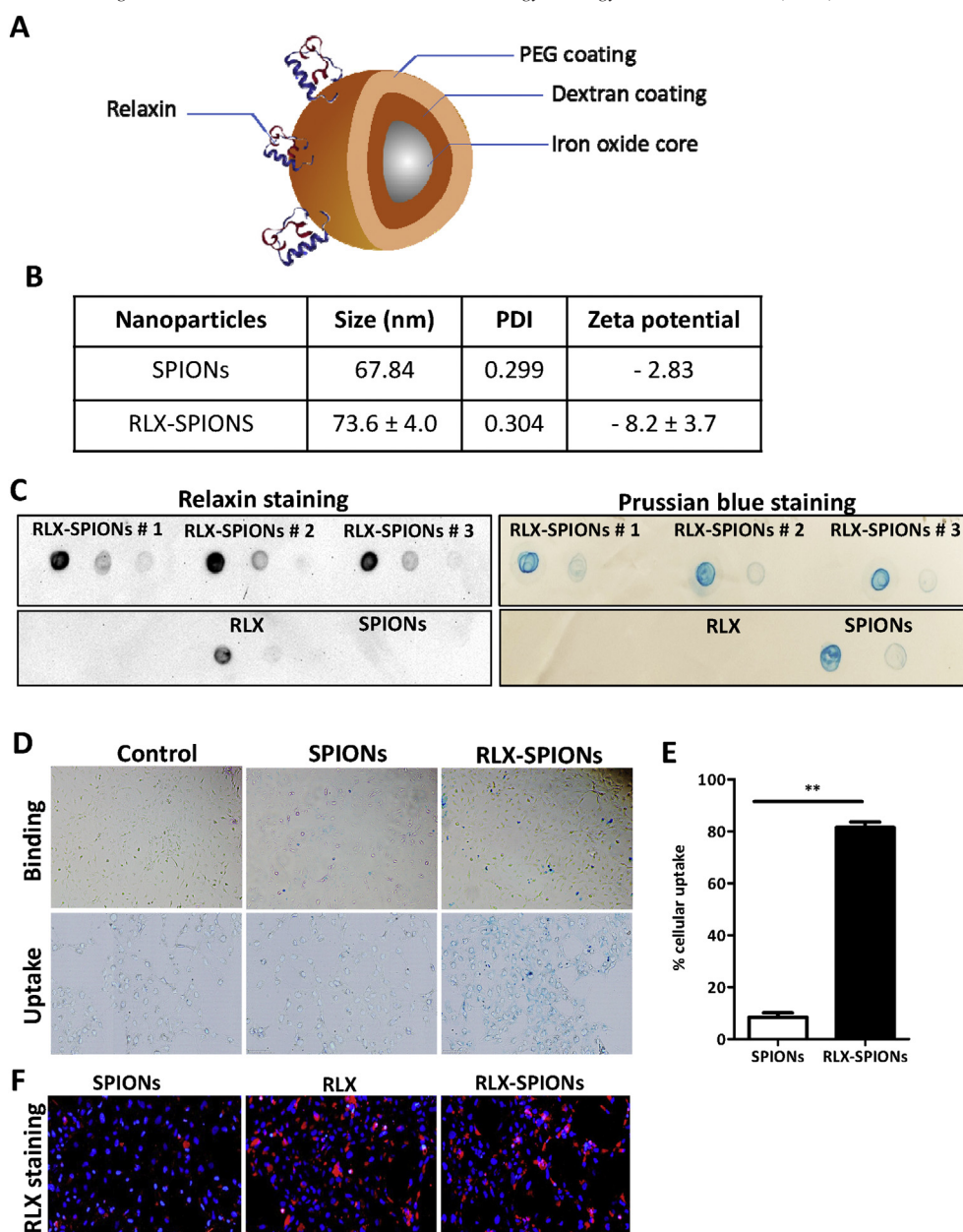


Figure 2. Characterization and HSC-specific binding/uptake of RLX-SPIONs. (A) Schematic representation of RLX-SPIONs. (B) Table showing the hydrodynamic size, polydispersity index (PDI) and zeta potential of SPIONs and RLX-SPIONs from  $n = 5$  preparations. (C) Dot-blot analysis showing RLX conjugation on SPIONs performed by RLX staining and SPIONs detection by Prussian blue iron staining. RLX-SPIONs, RLX and SPIONs were serially diluted and spotted on the membrane, so the different dots in the figure represents the serial dilutions of the respective samples. (D) Representative microscopic images showing binding and uptake of RLX-SPIONs versus SPIONs in TGF $\beta$ -activated LX2 cells. (E) Quantitative analysis depicting % cellular uptake of RLX-SPIONs versus SPIONs in TGF $\beta$ -activated LX2 cells,  $n = 3$ .  $**P < 0.01$  denotes significance versus SPIONs. (F) Representative images depicting binding of RLX and RLX-SPIONs following relaxin staining.

significantly higher MRI contrast with RLX-SPIONs as compared to untargeted SPIONs and control (RLX) (Figure 5, B) suggesting increased uptake and localization of RLX-SPIONs as compared to SPIONs. Furthermore, T2\* scanning maps showed the homogenous and uniform distribution of RLX-SPIONs in liver parenchyma. These results demonstrate molecular MR imaging targeting RXFP1 receptor on HSCs using RLX-SPIONs as promising nanoparticles for diagnosis of liver cirrhosis.

#### RLX-SPIONs ameliorated CCL<sub>4</sub>-induced liver cirrhosis in mice

We studied the therapeutic efficacy of RLX-SPIONs in 8-week CCL<sub>4</sub>-induced advanced and established liver cirrhosis model in vivo. This experimental model represents the clinical pathology of human liver cirrhosis. Briefly, mice received CCL<sub>4</sub> for 8 weeks to induce advanced liver cirrhosis/cirrhosis. During the last 2 weeks, six doses of vehicle, RLX, RLX-SPIONs or SPIONs were administered



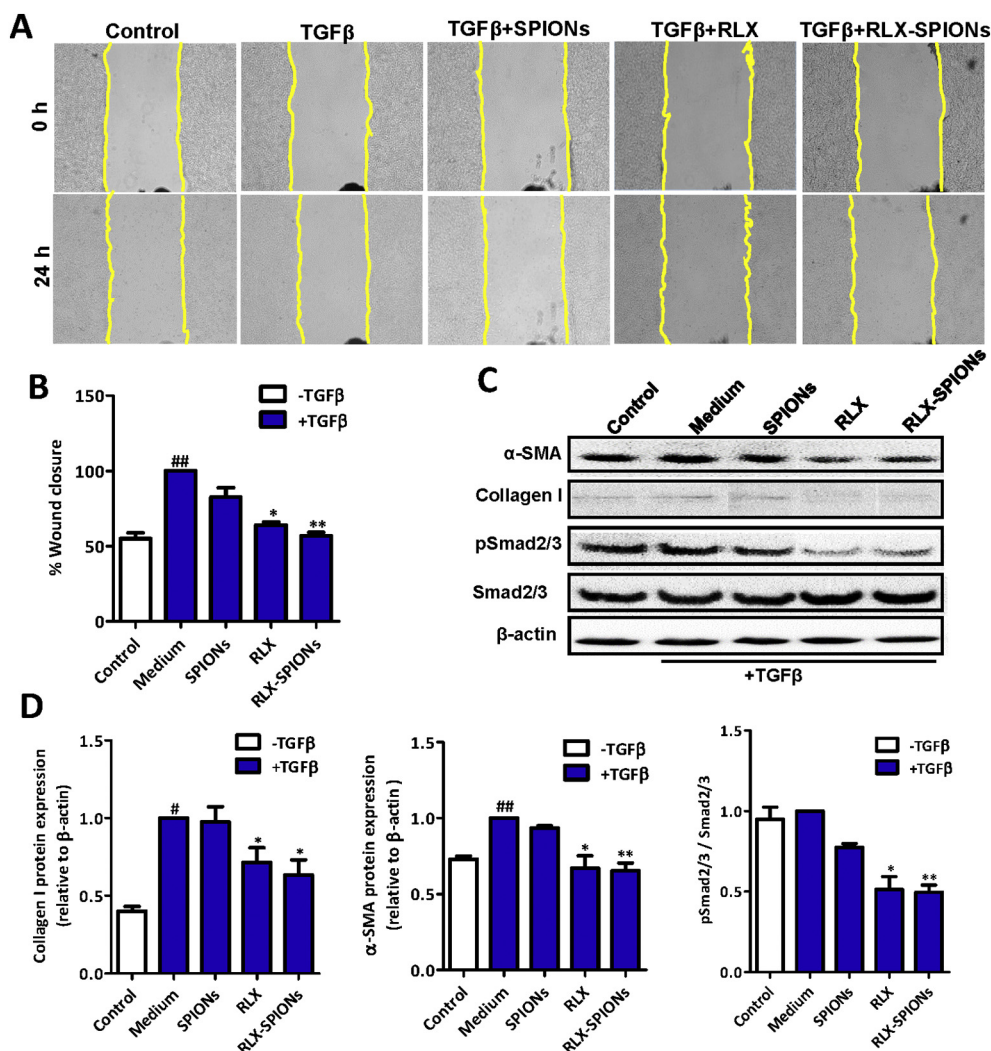


Figure 3. Efficacy of RLX-SPIONs in TGFβ-activated murine 3 T3 fibroblasts. (A) Representative images (n = 3) depicting scratch wounds made at 0 and wound closure at 24 h by control and TGFβ-stimulated 3 T3 fibroblasts treated with medium alone, SPIONs, RLX and RLX-SPIONs. (B) Graph showing % wound closure after 24 h, n = 3. (C) Representative images and (D) Quantitative analysis of western blot depicting bands for α-SMA, Collagen I, pSMAD2/3, SMAD2/3 and β-actin, performed on control and TGFβ-stimulated 3 T3 fibroblasts treated with medium alone, SPIONs, RLX and RLX-SPIONs, n = 3. <sup>#</sup>*P* < 0.05, <sup>##</sup>*P* < 0.01 denotes significance versus control 3 T3 cells and <sup>\*</sup>*P* < 0.05, <sup>\*\*</sup>*P* < 0.01 denotes significance versus TGFβ-treated 3 T3 fibroblasts.

intravenously (Figure 6, A) while continuing the CCl<sub>4</sub> administration which resembles the clinical treatment regimen. CCl<sub>4</sub> mice developed extensive bridging cirrhosis, substantial deposition of collagen I, and increased expression of the HSC marker, desmin (Figure 6, B). Correspondingly, mRNA expression of collagen I and HSC markers, α-SMA and TIMP1 were highly significantly induced in CCl<sub>4</sub> fibrotic mice (Figure 6, C). Interestingly, RLX and more significantly RLX-SPIONs inhibited the expression of these fibrotic markers (Figure 6B and C). We also analyzed serum alanine aminotransferase (ALT) levels and observed downregulation in ALT levels with RLX-SPIONs alone while other treatment did not influence CCl<sub>4</sub>-induced ALT levels (Supplementary Fig. 3, A). We also measured body weights of mice before and after treatments, and found that RLX reduced the body weight of the animals while RLX-SPIONs improved the body weights demonstrating reduced adverse effects (Supplementary Fig. 3, B). Notably, in line with our in vitro data, we did not observe any effect from SPIONs alone.

Additionally, as shown earlier that RLX has effects on matrix metalloproteinases (MMPs) expression and hence regulates collagen remodeling,<sup>30</sup> we have also analyzed influence of RLX-SPIONs on intrahepatic MMPs (MMP2, MMP3, MMP9 and MMP13). MMP2 and MMP13 are identified as pro-fibrotic MMPs, and MMP3 and MMP9 are defined as anti-fibrotic MMPs.<sup>31</sup> We found that RLX and more strongly RLX-SPIONs inhibited pro-fibrotic MMP2 and MMP13 expression (Figure 7, A) while induced anti-fibrotic MMP3 and MMP9 (Supplementary Fig. 4, A, B). Altogether, these results strongly suggest that RLX-SPIONs exhibited improved therapeutic efficacy without adverse effects.

#### RLX-SPIONs attenuated CCl<sub>4</sub>-induced angiogenesis and induced intrahepatic nitric oxide signaling

Angiogenesis induced by hypoxia within an injured liver and appears to aggravate hepatic fibrogenesis.<sup>32,33</sup> Accordingly, we

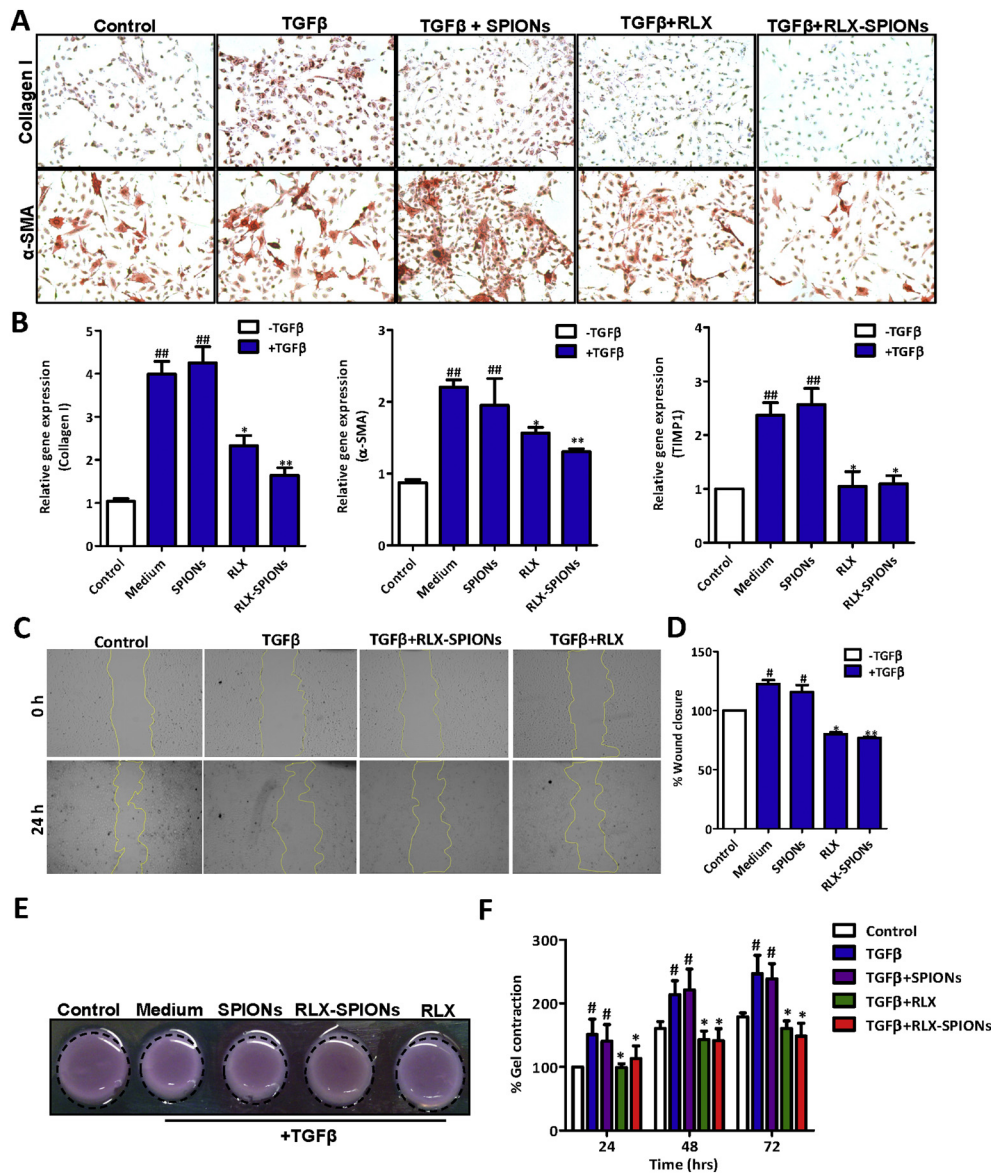


Figure 4. Efficacy of RLX-SPIONs in TGFβ-activated human HSCs (LX2). (A) Representative images ( $n = 3$ ) showing Collagen I- and α-SMA-stained control and TGFβ-activated LX2 treated with medium alone, SPIONs, RLX and RLX-SPIONs. (B) Gene expression analysis for Collagen I, α-SMA and TIMP1 as examined in control and TGFβ-activated LX2 cells treated with medium alone, SPIONs, RLX and RLX-SPIONs,  $n = 3$ . (C) Representative images (at 0 and 24 h) and (D) Quantitative analysis (after 24 h) of wound healing/migration by control and TGFβ-stimulated LX2 cells treated with medium alone, SPIONs, RLX and RLX-SPIONs (E) Representative images (after 72 h) and (F) quantitative analysis of 3D collagen I gel contraction containing control and TGFβ-activated LX2 treated with medium alone, SPIONs, RLX and RLX-SPIONs,  $n = 3$ . # $P < 0.05$  versus control HSCs; \* $P < 0.05$  and \*\* $P < 0.01$  versus TGFβ-treated HSCs.

observed significant increase in angiogenesis markers, endothelin-1, CD31 and CD34, and hypoxia induced factor 1 alpha (HIF1α) in the livers of mice chronically treated with CCl<sub>4</sub> (Figure 7, B–D and Supplementary Fig. 4,C). The intrahepatic expression of these angiogenesis markers were significantly inhibited following therapeutic treatment with RLX and more strongly with RLX-SPIONs (Figure 7, B–D and Supplementary Fig. 4,C). Since RLX has been shown to have role in portal hypertension mediated via nitric oxide pathway,<sup>8</sup> we also studied intrahepatic expression of nitric oxide synthases (NOS), nitric oxide synthases regulator caveolin-1 and serum levels of nitrite levels and found that RLN-SPIONs dramatically increased the expression levels of

NOS expression while decreased the expression of Caveolin-1 (Figure 7, E and F). These effects are highly significant as compared to RLX alone suggesting strong effects of RLX-SPIONs on portal hypertension. Notably, Endothelin-1, is also defined as contractile agonist, was also strongly inhibited following treatment with RLX-SPIONs (Figure 7, B) further demonstrating RLX-SPIONs effects on HSCs contractility and also in amelioration of portal hypertension.

To investigate the systemic effects of RLX-SPIONs versus RLX, we analyzed total nitrite levels in plasma. Interestingly, we found highly significant induction in systemic NO production with RLX as compared to RLX-SPIONs suggesting increased



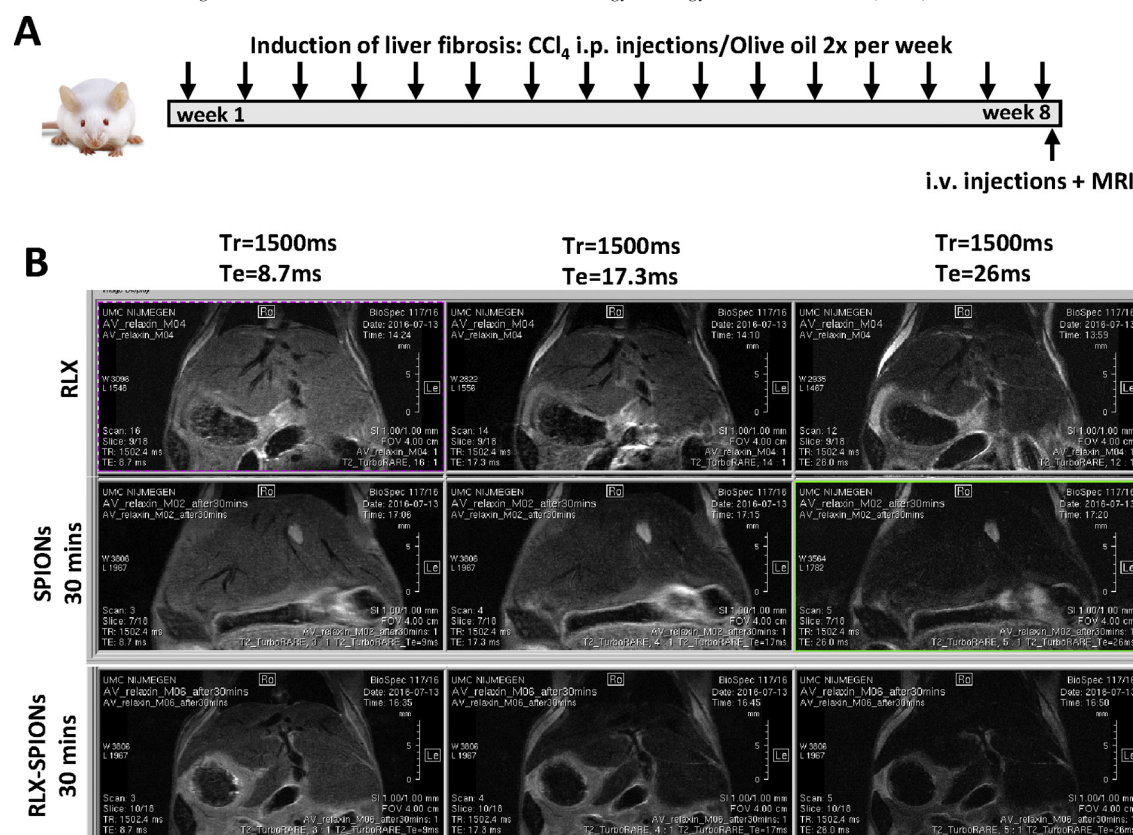


Figure 5. Magnetic resonance imaging of RLX-SPIONs in vivo in CCl<sub>4</sub>-induced liver cirrhosis mouse model. (A) Regimen of liver cirrhosis induction. After 8 weeks of CCl<sub>4</sub> injections, animals received RLX, SPIONs, RLX-SPIONs (5 µg/mice/dose) intravenously and MRI was performed after 30 min of intravenous administration. (B) T2 contrast-enhanced MRI liver scan performed on CCl<sub>4</sub>-induced liver fibrotic mice that RLX, SPIONs, RLX-SPIONs.

systemic effects of RLX due to multiple dosing and reduced adverse effects from RLX-SPIONs (Figure 7, H). Based on these results, we proposed that since RLX-SPIONs demonstrated increased liver uptake and distribution (Figure 5) and hence showed increased expression of intrahepatic NO synthases and exerted RLX-mediated localized effects within the fibrotic liver. However, free unconjugated RLX induced systemic effects and showed increased plasma nitrite levels as compared to RLX-SPIONs attributed to the comparatively reduced uptake in the liver. Altogether these results demonstrate the inhibitory effects of RLX-SPIONs in portal hypertension with no systemic effect on relaxant factor (NO) or vasodilation.

In vivo, we observed the improved therapeutic efficacy with RLX-SPIONs as compared to free RLX which might be due to (a) improved stability, (b) improved pharmacokinetics due to longer circulation and (c) multivalent interaction of RLX-SPIONs versus monovalent interaction of free RLX. Herein, we investigated the stability of RLX-SPIONs versus free RLX in serum in vitro. We performed the migration assay (scratch assay) and quantitative PCR analysis whereby RLX and RLX-SPIONs were incubated with TGFβ-activated LX2 cells in the absence and presence of serum (Supplementary Figs. 5 and 6). We observed that although RLX and RLX-SPIONs showed potent inhibitory effects in vitro in the absence of serum, however, RLX showed significantly reduced therapeutic efficacy as compared to RLX-SPIONs in the presence of serum (Supplementary

Figs. 5 and 6), strongly suggesting the improved stability of RLX-SPIONs and therefore, very likely, improved pharmacokinetic profile as compared to free RLX.

## Discussion

We have developed a novel theranostic nanomedicine by targeting relaxin (RLX) using SPIONs for the diagnosis and the treatment of liver cirrhosis. We demonstrate the SPIONs-based strategy to deliver potent therapeutic peptide hormone RLX specifically to relaxin receptor (RXFP1), that is overexpressed on HSCs (the key pathogenic cell types in liver), as a promising strategy for molecular magnetic resonance imaging and targeted therapy of liver cirrhosis. RLX-SPION showed specific binding and uptake by HSCs since RLX receptors are specifically overexpressed on activated HSCs during liver cirrhosis. Furthermore, RLX-SPIONs inhibited HSCs activation, migration and contractility demonstrating the multidimensional effect of RLX and that RLX activities were completely retained following chemical conjugation. In vivo, in advanced and established model of liver cirrhosis in mice, RLX-SPIONs showed increased MRI contrast as compared to SPIONs and increased therapeutic efficacy as compared to RLX alone. Importantly, RLX-SPIONs strongly inhibited ECM deposition, ECM remodeling, HSCs activation, angiogenesis and portal

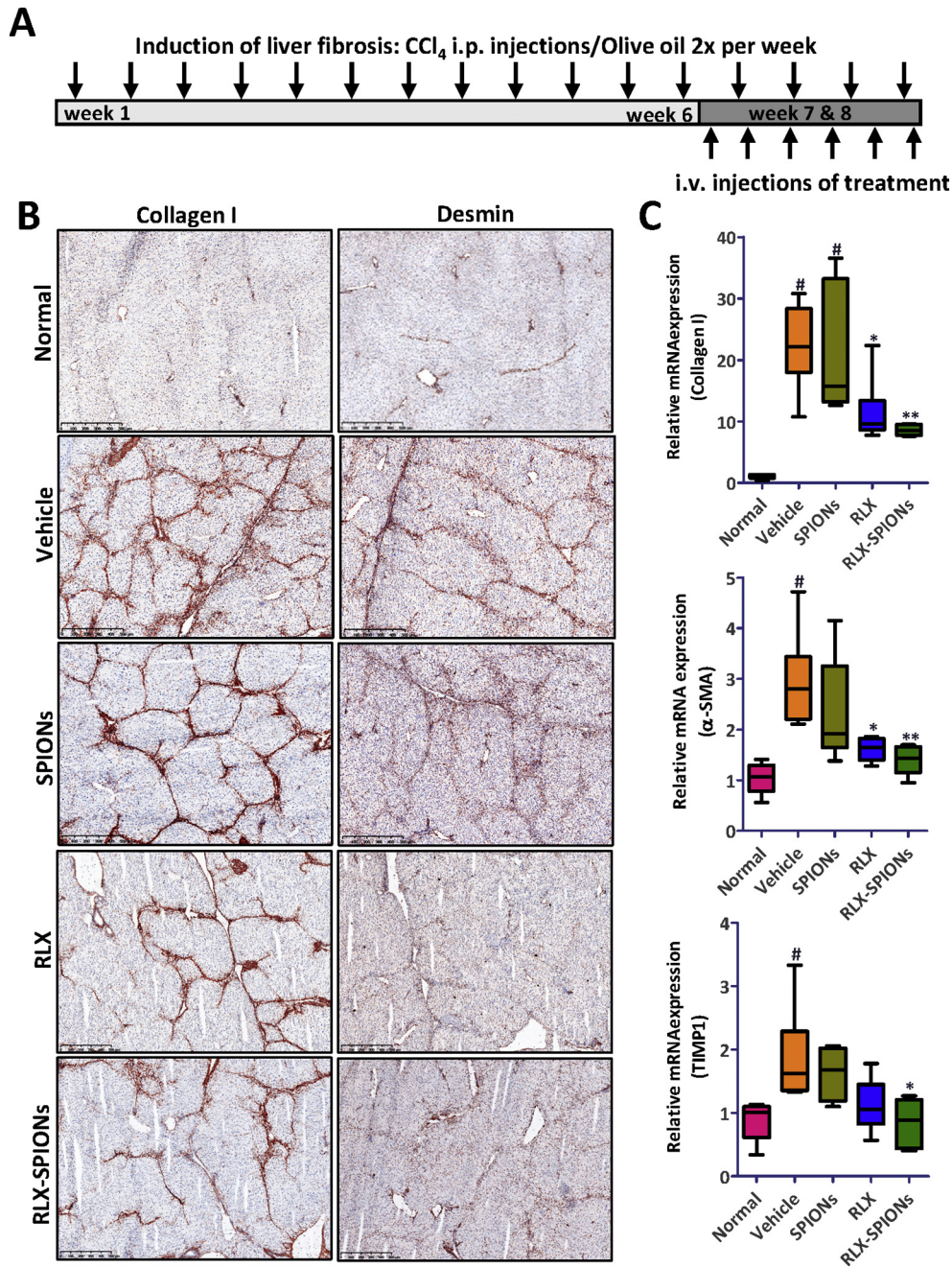


Figure 6. Effects of RLX-SPIONs on cirrhosis-related parameters in CCl<sub>4</sub>-treated fibrotic mice. (A) Regimen of liver cirrhosis induction. After 6 weeks of CCl<sub>4</sub> injections, animals received PBS (n = 6), RLX (250 ng/dose, n = 6), RLX-SPIONs (250 ng/dose, n = 6) and SPIONs (equimolar concentration as RLX-SPIONs, n = 5), 3 times a week intravenously for 2 weeks, while CCl<sub>4</sub> injections were continued. Normal healthy controls (n = 5) received olive oil for 8 weeks. (B) Representative photomicrographs of collagen I and desmin-stained liver sections of olive oil-treated animals (normal) and fibrotic animals treated with PBS, SPIONs, RLX and RLX-SPIONs. (C) Quantitative real-time PCR analysis of collagen I, α-SMA and TIMP1 in olive oil-treated mice (normal) and CCl<sub>4</sub> animals treated with PBS, SPIONs, RLX and RLX-SPIONs. Bars represent mean ± SEM, n = 5–6 mice per group. #P < 0.05 versus olive oil normal mice; \*P < 0.05, \*\*P < 0.01 versus PBS treated-CCl<sub>4</sub> mice.

hypertension. In contrast, RLX induced systemic adverse effects i.e. systemic vasodilation by release of relaxant factor i.e. nitric oxide and decreased the body weight in mice, while RLX-SPIONs did not show any side effects.

RLX is composed of chain A and B joint with a linker and it has been demonstrated that chain A is responsible for the biological activity.<sup>34</sup> Taking the advantage of RLX molecular

structure, we smartly conjugated one chain (chain B) of RLX to SPIONs while the other active chain (chain A) remained free to interact with RLX receptor. Since RLX needs to interact with the RXFP1 receptor present on the HSCs surface for the activation of the RLX signaling pathway and thereby inhibition of HSCs activation, we conjugated RLX (chain B) on the surface of SPIONs with a PEG spacer that allows RLX (chain A) to freely

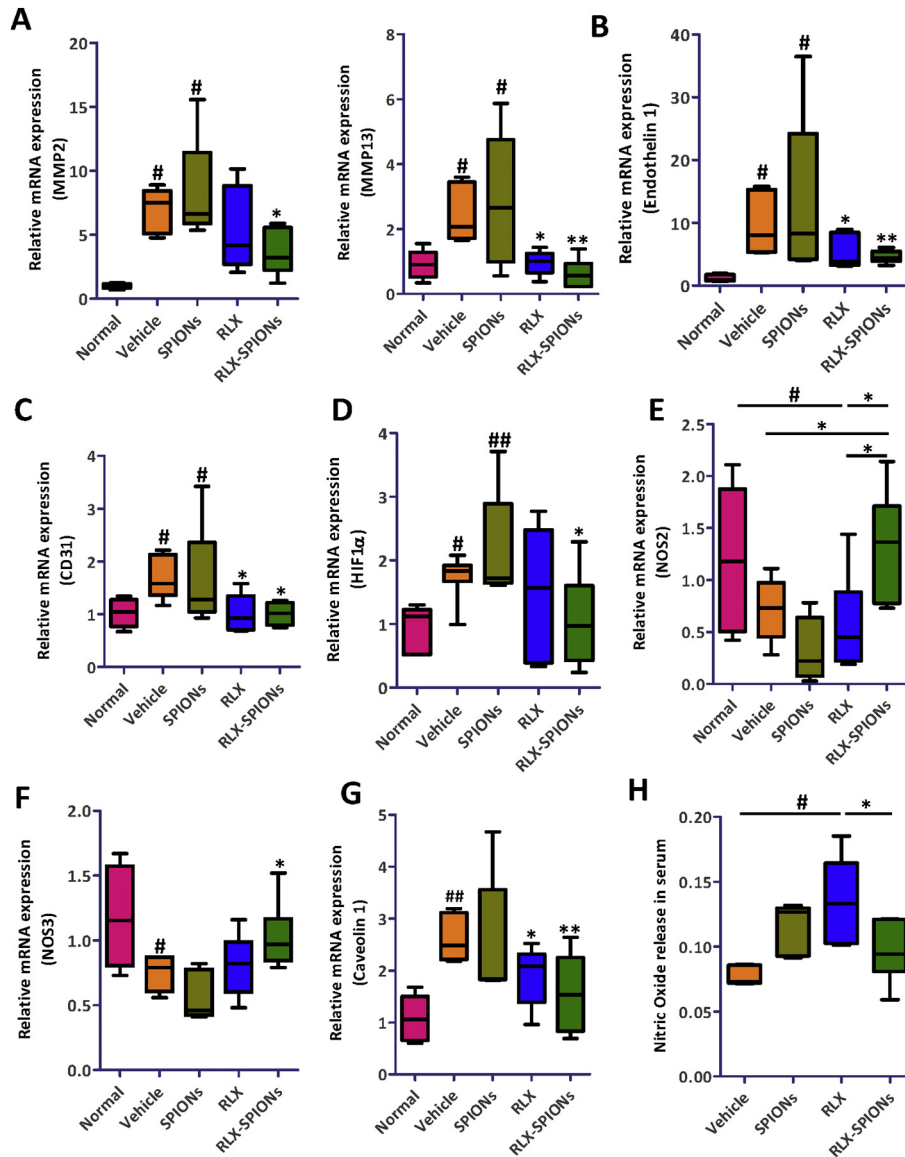


Figure 7. Effect of RLX-SPIONs on angiogenesis, MMPs, NO bioavailability and signaling in 8-week CCl<sub>4</sub> fibrotic mice. Hepatic mRNA expression of (A) MMP-2 and -13; angiogenesis markers (B) Endothelin 1, (C) CD31, and (D) HIF1α; Nitric oxide pathway markers (E) NOS2 (iNOS) and (F) NOS3 (eNOS), and (G) NOS3 regulator, Caveolin 1; and (H) Serum total nitrite levels as assessed in olive oil-treated mice (normal) and CCl<sub>4</sub> animals treated with PBS, SPIONs, RLX and RLX-SPIONs. Bars represent mean ± SEM, n = 5–6 mice per group. <sup>#</sup>*P* < 0.05, <sup>##</sup>*P* < 0.01 versus olive oil normal mice; <sup>\*</sup>*P* < 0.05, <sup>\*\*</sup>*P* < 0.01 versus PBS treated-CCl<sub>4</sub> mice.

bind to the receptor. It is important to comprehend that after conjugation, such a molecule can lose its biological activity due to conjugation at the receptor interaction site or steric hindrance caused by the conjugation. Interestingly, we found that chain B had 2 lysine groups and a N-terminal amine group, which we used for conjugating RLX to SPIONs via carbodiimide chemistry. This conjugation strategy therefore makes RLX (chain A) accessible for binding to the receptor while having RLX (chain B) yet bound to surface of the SPIONs. Our *in vitro* effect studies confirmed that RLX-SPIONs did not lose the activity after conjugation, and showed even better efficacy especially in the presence of serum, where the efficacy of RLX was significantly reduced. This might be due to increased

stability of RLX-SPIONs allowing longer duration of activity and/or confinement of the molecules allowing better interaction with the receptor. In addition, it is also known that multivalent interaction instead of monovalent interaction can result in stronger and more selective interaction.<sup>35</sup> Therefore, multivalency and stability of RLX in RLX-SPIONs might have contributed to the enhanced therapeutic effects.

Hepatic cirrhosis, characterized by extensive accumulation of extracellular matrix leading to scar tissue formation in the liver resulting in liver dysfunction and hepatocellular carcinoma.<sup>2</sup> Activated HSCs are the key pathogenic cells responsible for the production of abnormal fibrillar collagens in liver cirrhosis,<sup>36,37</sup> therefore targeted therapeutics to reverse these activated HSCs are



of great interest. An emerging concept is the direct delivery of anti-fibrotics to target HSCs using receptor-specific carriers to increase local drug concentrations while preventing deleterious effects on non-target cells or other organs.<sup>5,6,36–38</sup> HSCs are the major liver cells that express RXFP1 and in light of RXFP1 overexpression on HSCs in liver cirrhosis, previous studies have demonstrated the therapeutic potential of RLX (6KDa, peptide hormone) and more recently, small molecule RXFP1 agonists in liver diseases.<sup>8,11,26,39–42</sup> Furthermore, RLX has been implicated as potent anti-fibrotic therapy for kidney and cardiac cirrhosis.<sup>12–15,43–48</sup> In the liver, RLX has shown to lead to the dilation of sinusoids and changes in the contractility of activated HSCs or myofibroblasts.<sup>49,50</sup> In activated rat HSCs, RLX has shown to result in a decreased collagen deposition and synthesis, accompanied by reduced expression of TIMP1 and TIMP2.<sup>51</sup> Several signaling pathways have been shown to be activated by RLX in HSCs including cAMP, cGMP, NO and Akt and have been shown to be involved in the HSCs-specific inhibitory effects of RLX.<sup>8,52</sup> Further studies have suggested that RLX interaction with RXFP1 receptors results in the activation of the anti-fibrotic transcription factor PPAR $\gamma$  through cAMP, PKA, p38-MAPK and PPAR $\gamma$  coactivator protein 1 $\alpha$  (PGC1 $\alpha$ ).<sup>40</sup> Promisingly, Serelaxin, a recombinant form of human relaxin-2 (H2-RLX) relieved dyspnea, showed improvement in clinical outcomes and reduced mortality in acute heart failure patients in a Phase 3 trial.<sup>53</sup> However, when injected into patients, H2-RLX has shown to lose half of its activity within 10 min due to the degradation by blood enzymes and clearance by the kidney and liver.<sup>17,18</sup> For treatment of liver diseases, chronic administration of RLX i.e. continuous infusion would be required due to the short half-life which would be major obstacle for the clinical translation of RLX. To improve the half-life, systemic vasodilation, administration and for future application for magnetic resonance imaging, we synthesized RLX-coated superparamagnetic iron-oxide nanoparticles (RLX-SPIONs). In this study, we used dextran- and PEG-coated SPIONs, since these hydrophilic polymers increase blood circulation time of SPIONs and reduce non-specific interactions with macrophages and reticuloendothelial system, and hence reduce nanotoxicity.<sup>20</sup> Since RLX-SPIONs does not interact and phagocytosed by macrophages and reticuloendothelial system due to the receptor specificity (highly expressed on HSCs) and surface modification (dextran and PEG), therefore we did not observe any response of innate immune system in vivo. Altogether, we did not observe any toxic effects from RLX-SPIONs in vitro and in vivo suggesting safety profile of these nanoparticles and hence relevance for the future clinical application.

Early and precise stage diagnosis of liver cirrhosis can be extremely helpful in predicting the prognosis and therapeutic outcome. In spite of advancements in the field of non-invasive strategies, liver biopsy remain the gold standard for staging of liver cirrhosis. Several advanced MRI techniques (diffusion-weighted imaging) have been developed for accurate staging of cirrhosis,<sup>54</sup> however, these MRI-techniques provide indirect measurements and can be confounded by several factors.<sup>54</sup> Therefore, direct visualization of key pathogenic cells might be more accurate to evaluate degree of cirrhosis. Recently, molecular imaging has emerged to visualize, characterize and measure the biological process at the molecular and cellular

level.<sup>55</sup> Due to high spatial resolution and nonionizing radiations, MRI has potential for molecular imaging. In this study, RLX-SPIONs showed enhanced contrast and hence demonstrates the applicability for diagnosis of liver fibrosis. In addition, RLX-SPIONs significantly ameliorated liver fibrosis without inducing systemic adverse effects.

To our best knowledge, this is the first study highlighting the theranostic application of RLX and SPIONs in liver cirrhosis and documenting increased therapeutic effects of RLX while overcoming the adverse effects. This promising strategy should be further trailed in other fibrotic diseases and should be explored for the systematic evaluation of its theranostic potential for clinical applications.

## Appendix A. Supplementary data

Supplementary data to this article can be found online at <https://doi.org/10.1016/j.nano.2018.12.008>.

## References

- Wallace MC, Friedman SL, Mann DA. Emerging and disease-specific mechanisms of hepatic stellate cell activation. *Semin Liver Dis* 2015;**35**:107–18.
- Bataller R, Brenner DA. Liver fibrosis. *J Clin Invest* 2005;**115**:209–18.
- Hernandez-Gea V, Friedman SL. Pathogenesis of liver fibrosis. *Annu Rev Pathol* 2011;**6**:425–56.
- Poelstra K. Liver fibrosis in 2015: crucial steps towards an effective treatment. *Nat Rev Gastroenterol Hepatol* 2016;**13**:67–8.
- Bansal R, Prakash J, de Ruijter M, Beljaars L, Poelstra K. Peptide-modified albumin carrier explored as a novel strategy for a cell-specific delivery of interferon gamma to treat liver fibrosis. *Mol Pharm* 2011;**8**:1899–909.
- Bansal R, Prakash J, De Ruijter M, Poelstra K. Targeted recombinant fusion proteins of IFN $\gamma$  and mimetic IFN $\gamma$  with PDGF $\beta$  bicyclic peptide inhibits liver fibrogenesis in vivo. *PLoS One* 2014;**9**:e9878.
- Bansal R, Prakash J, Post E, Beljaars L, Schuppan D, Poelstra K. Novel engineered targeted interferon-gamma blocks hepatic fibrogenesis in mice. *Hepatology* 2011;**54**:586–96.
- Fallowfield JA, Hayden AL, Snowdon VK, Aucott RL, Stutchfield BM, Mole DJ, et al. Relaxin modulates human and rat hepatic myofibroblast function and ameliorates portal hypertension in vivo. *Hepatology* 2014;**59**:1492–504.
- Sasser JM. The emerging role of relaxin as a novel therapeutic pathway in the treatment of chronic kidney disease. *Am J Physiol Regul Integr Comp Physiol* 2013;**305**:R559–65.
- Feijoo-Bandin S, Aragon-Herrera A, Rodriguez-Penas D, Portoles M, Rosello-Lleti E, Rivera M, et al. Relaxin-2 in Cardiometabolic diseases: mechanisms of action and future perspectives. *Front Physiol* 2017;**8**:599.
- Bennett RG, Heimann DG, Singh S, Simpson RL, Tuma DJ. Relaxin decreases the severity of established hepatic fibrosis in mice. *Liver Int* 2014;**34**:416–26.
- Hewitson TD, Mookerjee I, Masterson R, Zhao C, Tregear GW, Becker GJ, et al. Endogenous relaxin is a naturally occurring modulator of experimental renal tubulointerstitial fibrosis. *Endocrinology* 2007;**148**:660–9.
- Samuel CS, Lekgabe ED, Mookerjee I. The effects of relaxin on extracellular matrix remodeling in health and fibrotic disease. *Adv Exp Med Biol* 2007;**612**:88–103.
- Lekgabe ED, Kiriazis H, Zhao C, Xu Q, Moore XL, Su Y, et al. Relaxin reverses cardiac and renal fibrosis in spontaneously hypertensive rats. *Hypertension* 2005;**46**:412–8.

15. Du XJ, Xu Q, Lekgabe E, Gao XM, Kiriazis H, Moore XL, et al. Reversal of cardiac fibrosis and related dysfunction by relaxin. *Ann N Y Acad Sci* 2009;**1160**:278–84.
16. Samuel CS, Zhao C, Yang Q, Wang H, Tian H, Tregear GW, et al. The relaxin gene knockout mouse: a model of progressive scleroderma. *J Invest Dermatol* 2005;**125**:692–9.
17. Chen SA, Perlman AJ, Spanski N, Peterson CM, Sanders SW, Jaffe R, et al. The pharmacokinetics of recombinant human relaxin in nonpregnant women after intravenous, intravaginal, and intracervical administration. *Pharm Res* 1993;**10**:834–8.
18. Chen SA, Reed B, Nguyen T, Gaylord N, Fuller GB, Mordenti J. The pharmacokinetics and absorption of recombinant human relaxin in nonpregnant rabbits and rhesus monkeys after intravenous and intravaginal administration. *Pharm Res* 1993;**10**:223–7.
19. Debrah DO, Novak J, Matthews JE, Ramirez RJ, Shroff SG, Conrad KP. Relaxin is essential for systemic vasodilation and increased global arterial compliance during early pregnancy in conscious rats. *Endocrinology* 2006;**147**:5126–31.
20. Lin MM, Kim HH, Kim H, Dobson J, Kim DK. Surface activation and targeting strategies of superparamagnetic iron oxide nanoparticles in cancer-oriented diagnosis and therapy. *Nanomedicine (Lond)* 2010;**5**:109–33.
21. Rosen JE, Chan L, Shieh DB, Gu FX. Iron oxide nanoparticles for targeted cancer imaging and diagnostics. *Nanomedicine* 2012;**8**:275–90.
22. Tassa C, Shaw SY, Weissleder R. Dextran-coated iron oxide nanoparticles: a versatile platform for targeted molecular imaging, molecular diagnostics, and therapy. *Acc Chem Res* 2011;**44**:842–52.
23. Frimpong RA, Hilt JZ. Magnetic nanoparticles in biomedicine: synthesis, functionalization and applications. *Nanomedicine (Lond)* 2010;**5**:1401–14.
24. Issa B, Obaidat IM, Albiss BA, Haik Y. Magnetic nanoparticles: surface effects and properties related to biomedicine applications. *Int J Mol Sci* 2013;**14**:21266–305.
25. Tanimoto A, Kuribayashi S. Application of superparamagnetic iron oxide to imaging of hepatocellular carcinoma. *Eur J Radiol* 2006;**58**:200–16.
26. McBride A, Hoy AM, Bamford MJ, Mossakowska DE, Ruediger MP, Griggs J, et al. In search of a small molecule agonist of the relaxin receptor RXFP1 for the treatment of liver fibrosis. *Sci Rep* 2017;**7**:10806.
27. Friedman SL. Mechanisms of hepatic fibrogenesis. *Gastroenterology* 2008;**134**:1655–69.
28. Inagaki Y, Okazaki I. Emerging insights into transforming growth factor beta Smad signal in hepatic fibrogenesis. *Gut* 2007;**56**:284–92.
29. Lemoine S, Cadoret A, El Mourabit H, Thabut D, Housset C. Origins and functions of liver myofibroblasts. *Biochim Biophys Acta* 2013;**1832**:948–54.
30. Samuel CS. Relaxin: antifibrotic properties and effects in models of disease. *Clin Med Res* 2005;**3**:241–9.
31. Giannandrea M, Parks WC. Diverse functions of matrix metalloproteinases during fibrosis. *Dis Model Mech* 2014;**7**:193–203.
32. Chaparro M, Sanz-Cameno P, Trapero-Marugan M, Garcia-Buey L, Moreno-Otero R. Mechanisms of angiogenesis in chronic inflammatory liver disease. *Ann Hepatol* 2007;**6**:208–13.
33. Amarapurkar AD, Amarapurkar DN, Vibhav S, Patel ND. Angiogenesis in chronic liver disease. *Ann Hepatol* 2007;**6**:170–3.
34. Hossain MA, Wade JD, Bathgate RA. Chimeric relaxin peptides highlight the role of the A-chain in the function of H2 relaxin. *Peptides* 2012;**35**:102–6.
35. Kauscher U, Ravoo BJ. Mannose-decorated cyclodextrin vesicles: the interplay of multivalency and surface density in lectin-carbohydrate recognition. *Beilstein J Org Chem* 2012;**8**:1543–51.
36. Bansal R, Nagorniowicz B, Prakash J. Clinical advancements in the targeted therapies against liver fibrosis. *Mediators Inflamm* 2016;**2016**, 7629724.
37. Yazdani S, Bansal R, Prakash J. Drug targeting to myofibroblasts: implications for fibrosis and cancer. *Adv Drug Deliv Rev* 2017;**121**:101–16.
38. Bansal R, Prakash J, De Ruiter M, Poelstra K. Interferon gamma peptidomimetic targeted to hepatic stellate cells ameliorates acute and chronic liver fibrosis in vivo. *J Control Release* 2014;**179**:18–24.
39. Chen CZ, Southall N, Xiao J, Marugan JJ, Ferrer M, Hu X, et al. Identification of small-molecule agonists of human relaxin family receptor 1 (RXFP1) by using a homogenous cell-based cAMP assay. *J Biomol Screen* 2013;**18**:670–7.
40. Singh S, Simpson RL, Bennett RG. Relaxin activates peroxisome proliferator-activated receptor gamma (PPARgamma) through a pathway involving PPARgamma coactivator 1alpha (PGC1alpha). *J Biol Chem* 2015;**290**:950–9.
41. Xiao J, Chen CZ, Huang Z, Agoulnik IU, Ferrer M, Southall N, et al. *Discovery, Optimization, and Biological Activity of the First Potent and Selective Small-Molecule Agonist Series of Human Relaxin Receptor 1 (RXFP1)*. Bethesda (MD): Probe Reports from the NIH Molecular Libraries Program; 2010.
42. Xiao J, Huang Z, Chen CZ, Agoulnik IU, Southall N, Hu X, et al. Identification and optimization of small-molecule agonists of the human relaxin hormone receptor RXFP1. *Nat Commun* 2013;**4**:1953.
43. Bathgate RA, Lekgabe ED, McGuane JT, Su Y, Pham T, Ferraro T, et al. Adenovirus-mediated delivery of relaxin reverses cardiac fibrosis. *Mol Cell Endocrinol* 2008;**280**:30–8.
44. Samuel CS, Hewitson TD, Unemori EN, Tang ML. Drugs of the future: the hormone relaxin. *Cell Mol Life Sci* 2007;**64**:1539–57.
45. Xu Q, Lekgabe ED, Gao XM, Ming Z, Tregear GW, Dart AM, et al. Endogenous relaxin does not affect chronic pressure overload-induced cardiac hypertrophy and fibrosis. *Endocrinology* 2008;**149**:476–82.
46. Du XJ, Bathgate RA, Samuel CS, Dart AM, Summers RJ. Cardiovascular effects of relaxin: from basic science to clinical therapy. *Nat Rev Cardiol* 2010;**7**:48–58.
47. Samuel CS, Royce SG, Hewitson TD, Denton KM, Cooney TE, Bennett RG. Anti-fibrotic actions of relaxin. *Br J Pharmacol* 2017;**174**:962–76.
48. Wang C, Kemp-Harper BK, Kocan M, Ang SY, Hewitson TD, Samuel CS. The anti-fibrotic actions of Relaxin are mediated through a NO-sGC-cGMP-dependent pathway in renal Myofibroblasts in vitro and enhanced by the NO donor, Diethylamine NONOate. *Front Pharmacol* 2016;**7**:91.
49. Bani D, Nistri S, Quattrone S, Bigazzi M, Bani Sacchi T. The vasorelaxant hormone relaxin induces changes in liver sinusoid microcirculation: a morphologic study in the rat. *J Endocrinol* 2001;**171**:541–9.
50. Bani D, Nistri S, Quattrone S, Bigazzi M, Sacchi TB. Relaxin causes changes of the liver. In vivo studies in rats. *Horm Metab Res* 2001;**33**:175–80.
51. Bennett RG, Kharbada KK, Tuma DJ. Inhibition of markers of hepatic stellate cell activation by the hormone relaxin. *Biochem Pharmacol* 2003;**66**:867–74.
52. Bennett RG, Dalton SR, Mahan KJ, Gentry-Nielsen MJ, Hamel FG, Tuma DJ. Relaxin receptors in hepatic stellate cells and cirrhotic liver. *Biochem Pharmacol* 2007;**73**:1033–40.
53. Teerlink JR, Cotter G, Davison BA, Felker GM, Filippatos G, Greenberg BH, et al. Serelaxin, recombinant human relaxin-2, for treatment of acute heart failure (RELAX-AHF): a randomised, placebo-controlled trial. *Lancet* 2013;**381**:29–39.
54. Talwalkar JA, Yin M, Fidler JL, Sanderson SO, Kamath PS, Ehman RL. Magnetic resonance imaging of hepatic fibrosis: emerging clinical applications. *Hepatology* 2008;**47**:332–42.
55. Li Z, Sun J, Yang X. Recent advances in molecular magnetic resonance imaging of liver fibrosis. *Biomed Res Int* 2015;**2015**:595467.